Optimization of a GaN-based irregular multiple quantum well structure for a dichromatic white LED*

Lu Hui-Min(路慧敏)† and Chen Gen-Xiang(陈根祥)

Institute of Lightwave Technology, Beijing Jiaotong University, Beijing 100044, *China*

(Received 12 March 2010; revised manuscript received 26 November 2010)

GaN-based irregular multiple quantum well (IMQW) structures assembled two different types of QWs emitting complementary wavelengths for dichromatic white light-emitting diodes (LEDs) are optimized in order to obtain near white light emissions. The hole distributions and spontaneous emission spectra of the IMQW structures are analysed in detail by fully considering the effects of strain, well-coupling, valence band-mixing and polarization effect through employing a newly developed theoretical model from the $\boldsymbol{k}\cdot\boldsymbol{p}$ theory. Several structure parameters such as well material component, well width, layout of the wells and the thickness of barrier between different types of QWs are employed to analyse how these parameters together with the polarization effect influence the electronic and the optical properties of IMQW structure. Numerical results show that uniform hole distributions in different types of QWs are obtained when the number of the QWs emitting blue light is two, the number of the QWs emitting yellow light is one and the barrier between different types of QWs is 8nm in thickness. The near white light emission is realized using GaN-based IMQW structure with appropriate design parameters and injection level.

Keywords: irregular multiple quantum wells, GaN-based, white LED

PACS: 78.67.De, 78.66.Fd, 78.81.Ey **DOI:** 10.1088/1674-1056/20/3/037807

1. Introduction

With recent breakthroughs in material growth and device fabrication technologies, GaN-based light-emitting diodes (LEDs) have made tremendous progress. The GaN-based white LEDs have attracted more and more attention for their many applications such as backlight of liquid crystal display panels, white light wireless communication and illumination light replacing bumps or even daylight lamps. Commercial white LEDs are usually fabricated using blue LED covered by a phosphor absorbing part of the blue or UV light and re-emitting yellow, Green/Red or Blue/Green/Red light.[1−5] The other common method is multi-chip LEDs composed of more than two different colour LEDs whose emissions can be combined to generate white light. However, the phosphors covered LEDs encounter lower efficiency and environmental issues and the multi-chip LEDs have the disadvantages of process complication, short lifetime and high cost. As result, many approaches to the fabrication of single-chip white LEDs without using phosphors have been proposed. In the photon recycling LED a fraction of the light emitted by the blue LED is absorbed by the A1GaInP active region and recycles the light with complementary colour.[6] In Ref. [7], the stable and near visible white light emissions can be generated by combining dual-wavelength GaN-based MQWs with the transverse p-n junction. Other techniques, such as laterally distributed InGaN/GaN MQW LEDs[8] and Si and Zn codoped InGaN/GaN MQW LEDs,[9] were also proposed.

GaN-based irregular multiple quantum well (IMQW) structures can also realize the phosphor-free single-chip white LEDs which have been reported in our previous work.[10] For the dichromatic white LED the IMQW structure is composed of two different types of QWs emitting complementary monochromatic wavelengths. The IMQW structure for the trichromatic white LED is assembled by three different types of QWs emitting blue, green, and red light. White light is expected from the mixtures of different colour light with an appropriate ratio. In the present study, the IMQW structure for dichromatic white LED is optimized by adjusting the design parameters, such as well material components, well width, layouts of the different types of QWs, and the thickness of barrier between different QWs in or-

*Project supported by the National Natural Science Foundation of China (Grant No. 60777013), the Nature Science Foundation of Beijing, China (Grant No. 4082023), and the Excellent Doctoral Science and Technology Innovation Foundation of Beijing Jiaotong University, China (Grant No. 141063522).

†Corresponding author. E-mail: luhuimin@china.com.cn

© 2011 Chinese Physical Society and IOP Publishing Ltd

der to obtain white light emission. Polarization effect plays a major role in determining the electronic and the optical properties of GaN-based IMQW structures due to the polarization-induced built-in electrostatic fields.[11−13] The carrier distributions and spontaneous emission spectra of the IMQW structures with different structure parameters are systematically analysed using the simulation program which we have written based on a detailed theoretical model by fully considering the effects of strain, well-coupling, valence band-mixing and polarization effect. Near white light emission is obtained by optimizing the structure parameters of IMQW structure for dichromatic white LED.

2. Theoretical model

The effective-mass Hamiltonian deduced from the $\boldsymbol{k}\cdot\boldsymbol{p}$ method is employed for calculating the electronic band structures and the optical gain spectra of (0001) oriented, the strained wurtzite GaN single quantum well (SQW) structure.[14−17] In the present work, the classical theoretical model is modified in order to obtain the electronic and the optical properties of the IMQW structure with considering the polarization effect. The effects of strain, well-coupling, valence band-mixing and polarization effect are fully considered in our theoretical model.

The coupling between the conduction band and the valence band is ignored due to the large band gaps of GaN material system, and the valence band structures are calculated using six-by-six effective-mass Hamiltonian. For the conduction band the subband energies $E_n^{\mathrm{c}}(k_t)$ and associated envelope function $h_n(z;k_t)$ are determined by solving the following effective mass equation expressed as

$$\left[\frac{\hbar^2}{2}\left(\frac{k_t^2}{m_{\mathrm{e}}^t}+\frac{k_z^2}{m_{\mathrm{e}}^z}\right)+E_{\mathrm{c}}(z)\right]h_n(z;k_t) = E_n^{\mathrm{c}}(k_t)\,h_n(z;k_t). \tag{1}$$

The total potential profile $E_{\mathrm{c}}(z)$ for the conduction band is

$$E_{\mathrm{c}}(z)=E_{\mathrm{c}}^0(z)+P_{\mathrm{c}\varepsilon}(z)+|e|\,Ez-|e|\,\phi(z), \tag{2}$$

where $E_{\mathrm{c}}^0(z)$ is the unstrained conduction band edge, $P_{\mathrm{c}\varepsilon}(z)$ is the hydrostatic energy shift in the conduction band induced by mechanical stresses, $|e|\,Ez$ denotes the additional Hamiltonian term due to the spontaneous polarization (SP) and the piezoelectric (PZ) polarization, and $\phi(z)$ is the electrostatic potential which satisfies Poisson equation. For a strained-layer wurtzite crystal grown along the (0001) oriented substrate, $P_{\mathrm{c}\varepsilon}(z)$ is given by

$$P_{\mathrm{c}\varepsilon}(z)=2\left(a_{\mathrm{ct}}-a_{\mathrm{cz}}\frac{C_{13}}{C_{33}}\right)\varepsilon_{xx}, \tag{3}$$

where a_{ct} and a_{cz} are the conduction band hydrostatic deformation potentials, C_{13} and C_{33} are the stiffness constants, and ε_{xx} is the diagonal element of the strain tensor. In MQW structure the electric field inside j-th layer is given by

$$E_j=(D-P_j)/\varepsilon_j, \tag{4}$$

where D is the displacement field, P_j is the total polarization including SP and PZ and ε_j is static dielectric constant in layer j. Using the condition of zero average electric field in the MQW region, the displacement field can be expressed as[13]

$$D=\frac{\sum\limits_k l_kP_k/\varepsilon_k}{\sum\limits_k l_k/\varepsilon_k}, \tag{5}$$

where l_k is the thickness of the k-th layer. It should be noted that if polarization effects are taken into account, the sign of the barrier field will be opposite to that of the well so that the square confinement potential will change into triangle potential.

For the valence band, the six-by-six Hamiltonian can be block-diagonalzed[14]

$$H_{6\times6}^{\mathrm{v}}(k)=\begin{bmatrix}H_{3\times3}^{\mathrm{U}}(k) & 0\\ 0 & H_{3\times3}^{\mathrm{L}}(k)\end{bmatrix}, \tag{6}$$

where $H^{\mathrm{U}}=\left(H^{\mathrm{L}}\right)^*$ and H^{U} is defined as

$$H^{\mathrm{U}}=\begin{bmatrix}F & K_t & -\mathrm{i}\,H_t\\ K_t & G & \Delta-\mathrm{i}\,H_t\\ \mathrm{i}\,H_t & \Delta+\mathrm{i}\,H_t & \lambda\end{bmatrix}, \tag{7}$$

$$\begin{aligned}&F=\Delta_1+\Delta_2+\lambda+\theta,\quad G=\Delta_1-\Delta_2+\lambda+\theta,\\ &\lambda=\frac{\hbar^2}{2m_0}\left(A_1k_z^2+A_2k_t^2\right)+D_1\varepsilon_{zz}+D_2\left(\varepsilon_{xx}+\varepsilon_{yy}\right),\\ &\theta=\frac{\hbar^2}{2m_0}\left(A_3k_z^2+A_4k_t^2\right)+D_3\varepsilon_{zz}+D_4\left(\varepsilon_{xx}+\varepsilon_{yy}\right),\\ &K_t=\frac{\hbar^2}{2m_0}A_5k_t^2,\quad H_t=\frac{\hbar^2}{2m_0}A_6k_zk_t,\\ &\Delta=\sqrt{2}\Delta_3,\end{aligned} \tag{8}$$

where A_is are the valence-band effective-mass parameters, Δ_1 is the crystal-field split energy, Δ_2 and Δ_3 are the spin-orbit split-off energies, and D_is are the deformation potentials. The valence-subband structure for

the upper Hamiltonian $E_m^{\mathrm{U}}(k_t)$ and the corresponding envelope functions $g_m^{(j)}(z;k_t)$ can be determined by solving the following effective equation:

$$\sum_j^3 \left(H_{ij}^{\mathrm{U}} \left(k_t; k_z = -\mathrm{i}\frac{\partial}{\partial z} \right) + \delta_{ij} E_{\mathrm{v}}(z) \right) g_m^{(j)}(z;k_t) = E_m^{\mathrm{U}}(k_t)\, g_m^{(j)}(z;k_t). \quad (9)$$

The total potential profile for the valence band $E_{\mathrm{v}}(z)$ is

$$E_{\mathrm{v}}(z) = E_{\mathrm{v}}^0(z) + |e| Ez - |e|\phi(z), \quad (10)$$

where $E_{\mathrm{v}}^0(z)$ is the unstrained valence band edge.

The electron and the hole density distributions in an active region are given respectively by

$$n(z) = \frac{1}{\pi} \sum_n \int_0^\infty k_t \mathrm{d}k_t f_n^{\mathrm{c}}(k_t) |h_n|^2$$

and

$$p(z) = \frac{1}{\pi} \sum_m \int_0^\infty k_t \mathrm{d}k_t f_m^{\mathrm{v}}(k_t) \times \left(\left| g_m^{(1)} \right|^2 + \left| g_m^{(2)} \right|^2 + \left| g_m^{(3)} \right|^2 \right), \quad (11)$$

where $f_n^{\mathrm{c}}(k_t)$ and $f_m^{\mathrm{v}}(k_t)$ are Fermi-Dirac distributions for the electrons in the conduction and for the hole in the valence bands, given by

$$f_n^{\mathrm{c}}(k_t) = \frac{1}{1 + \exp\left(\dfrac{E_n^{\mathrm{c}}(k_t) - F_{\mathrm{c}}}{\kappa_{\mathrm{B}} T} \right)}$$

and

$$f_m^{\mathrm{v}}(k_t) = \frac{1}{1 + \exp\left(\dfrac{E_m^{\mathrm{v}}(k_t) - F_{\mathrm{v}}}{\kappa_{\mathrm{B}} T} \right)}, \quad (12)$$

where F_{c} and F_{v} are the quasi-Fermi levels for electrons and holes, respectively.

For the upper Hamiltonians the momentum matrix elements $\left| (M_{\mathrm{e}})_{nm}^{\mathrm{U}}(k_t) \right|^2$ can be expressed as for $e = x$ and z

$$\left| (M_x)_{nm}^{\mathrm{U}}(k_t) \right|^2 = \frac{1}{4} \left(\left| \int_{-\infty}^{\infty} \mathrm{d}z h_n^* \langle S | p_x | X \rangle g_m^{(1)} \right|^2 + \left| \int_{-\infty}^{\infty} \mathrm{d}z h_n^* \langle S | p_x | X \rangle g_m^{(2)} \right|^2 \right),$$

$$\left| (M_z)_{nm}^{\mathrm{U}}(k_t) \right|^2 = \frac{1}{2} \left| \int_{-\infty}^{\infty} \mathrm{d}z h_n^* \langle S | p_z | X \rangle g_m^{(3)} \right|^2, \quad (13)$$

where the band-edge momentum matrix elements are obtained from Ref. [15] to be

$$|\langle S | p_x | X \rangle|^2 = \frac{m_0}{2} \left(\frac{m_0}{m_{\mathrm{e}}^t} - 1 \right) \frac{E_{\mathrm{g}} \left[(E_{\mathrm{g}} + \Delta_1 + \Delta_2)(E_{\mathrm{g}} + 2\Delta_2) - 2\Delta_3^2 \right]}{(E_{\mathrm{g}} + \Delta_1 + \Delta_2)(E_{\mathrm{g}} + \Delta_2) - \Delta_3^2},$$

$$|\langle S | p_z | X \rangle|^2 = \frac{m_0}{2} \left(\frac{m_0}{m_{\mathrm{e}}^z} - 1 \right) \frac{(E_{\mathrm{g}} + \Delta_1 + \Delta_2)(E_{\mathrm{g}} + 2\Delta_2) - 2\Delta_3^2}{(E_{\mathrm{g}} + 2\Delta_2)}. \quad (14)$$

The expressions of momentum matrix elements in this work are different from those obtained from the theoretical model in Ref. [15] because the band-edge matrix element varies with position for the spatially varying effective mass and energy parameters in the IMQW structure. The momentum matrix elements for the lower and the upper Hamiltonians have almost the same values although the IMQW is not of reflection symmetry structure and can be expressed as $|(M_{\mathrm{e}})_{nm}(k_t)|^2$ in a unified form. The final expression for spontaneous emission rate per unit volume per unit energy interval ($\mathrm{s}^{-1}\cdot\ \mathrm{cm}^{-3}\cdot\mathrm{eV}^{-1}$) can be written as

$$r_{\mathrm{sp}}(\hbar\omega) = \left(\frac{4 n_{\mathrm{r}} q^2 \omega}{\pi \hbar c^3 \varepsilon_0 m_0^2 L_z} \right) \sum_{n,m} \int \frac{k_t \mathrm{d}k_t}{6\pi} \left(2 |(M_x)_{nm}(k_t)|^2 + |(M_z)_{nm}(k_t)|^2 \right) \times \frac{\Gamma/(2\pi)}{\left(E_{nm}^{\mathrm{cv}}(k_t) - h\omega \right)^2 + (\Gamma/2)^2} f_n^{\mathrm{c}}(k_t)\left(1 - f_m^{\mathrm{v}}(k_t)\right), \quad (15)$$

where Γ is the linewidth of the Lorentzian function, and the expression

$$E_{nm}^{\mathrm{cv}}(k_t) = E_n^{\mathrm{c}}(k_t) - E_m^{\mathrm{v}}(k_t) \quad (16)$$

is the interband energy of the conduction band and valence band.

The parameters for wurtzites GaN and InN are listed in Table 1 and the parameters of InGaN are obtained using Vegard's law and appropriate bowing parameters.[14,18−21]

Table 1. Parameters for wurtzites GaN and InN.

parameters	GaN	InN
lattice constants/nm[a,b]		
a at 300 K	0.3189	0.3545
c at 300 K	0.5185	0.5703
energy parameters/eV[c,b]		
E_g at 300 K	3.392	0.744
$\Delta_1 = \Delta_{cr}$	0.019	0.041
$3\Delta_2 = 3\Delta_3 = \Delta_{so}$	0.014	0.001
$E_v^0(z)$	–2.64	–1.59
electron effective masses		
m_e^t/m_0	0.20	0.12
m_e^z/m_0	0.20	0.12
hole effective masses parameters [a,d]		
A_1	–6.56	–8.21
A_2	–0.91	–0.68
A_3	5.65	7.57
A_4	–2.83	–5.23
A_5	–3.13	–5.11
A_6	–4.86	–5.96
deformation potential/eV (this work)		
a_{ct}	–6.5	–3.5
a_{cz}	–11.8	–3.5
D_1	–3.0	–3.0
D_2	3.6	3.6
D_3	8.82	8.82
D_4	–4.41	–4.41
stiffness constants/GPa[d]		
C_{13}	106	92
C_{33}	398	224

[a]from Ref. [14], [b]from Ref. [19].
[c]from Ref. [20], [d]from Ref. [21].

3. Simulation result and discussion

According to the above-mentioned theoretical model, several structure parameters such as well material component, well width, layouts of the different types of QWs and the thickness of barrier between different QWs, were employed to study how these parameters change the carrier distribution and spontaneous emission spectrum of the IMQW structure. Nearly white light emission was obtained by optimizing the structure parameters of IMQW structure for dichromatic white LED.

3.1. Material components and width of well

The IMQW structure for the dichromatic white LED is assembled by two different types of QWs emitting complementary monochromatic wavelengths with a certain intensity ratio which can mix up to generate white light. First of all, the material components of the well layers were chosen in order to satisfy the band gap energy conditions for emitting complementary blue and yellow light, respectively. Due to the quantum effects, the emission spectrum of the MQW structure is sensitive to well width, which can also be used as an optimization parameter. Figure 1 shows the peak emission wavelengths of the MQW structures with different well material compositions for 2 nm well width and different well widths, with the same well material selected as $In_{0.2}Ga_{0.8}N$. GaN was selected as the barrier material and the thicknesses of barriers are all taken to be 8 nm for simplifying the simulation.

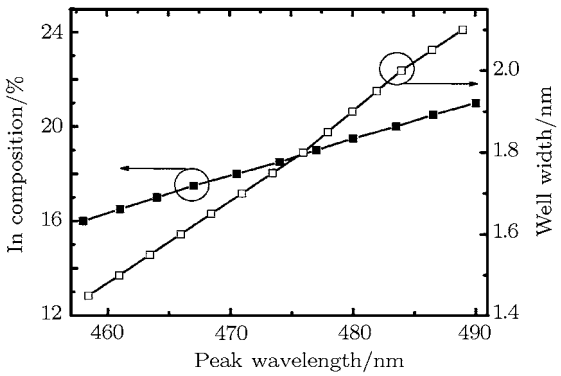


Fig. 1. Peak emission wavelengths of blue MQW for different well material compositions and well widths.

For white light mixing, 485 nm and 585 nm can be chosen as the peak emission wavelengths of the blue and the yellow light from MQW structure, respectively. If the above two complementary wavelength light mix to yield an overall emission with a certain intensity ratio, they will give the perception of white light. It can be obtained from the simulation result shown in Fig. 1 that the $In_{0.2}Ga_{0.8}N$/GaN MQW with 2 nm well width, whose spontaneous emission spectra are plotted in Fig. 2, has a 485 nm peek emission wavelength and accords with the above blue light emission condition. Similarly, the yellow light emission having a 585 nm peek wavelength can be obtained by the $In_{0.3}Ga_{0.7}N$/GaN MQW with a 2 nm well width, whose spontaneous emission spectra are also plotted in Fig. 2. For the $In_{0.3}Ga_{0.7}N$/GaN MQW the spontaneous emission spectra under different injection levels given in Fig. 2 are very different from each other, which can be explained by the carrier distribution.

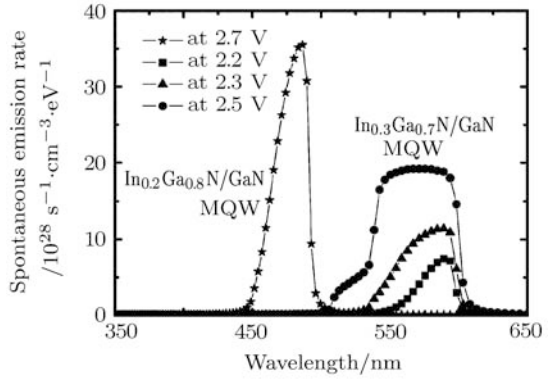


Fig. 2. Spontaneous emission rates of blue and yellow MQWs at different injection levels.

Figure 3 shows the hole distributions of the $In_{0.3}Ga_{0.7}N$/GaN MQW with two QWs under 2.2 V and 2.5 V applied to different subbands shown in Fig. 3(a) and different QWs plotted in Fig. 3(b). There are more holes distributed in light hole (LH) band at higher injection levels, which will lead to the broadening of spontaneous emission spectrum for the MQW structure. In addition, the nonuniform distributions of the holes in different QWs can also influence the spontaneous emission spectra of the MQW structures at different injection levels.

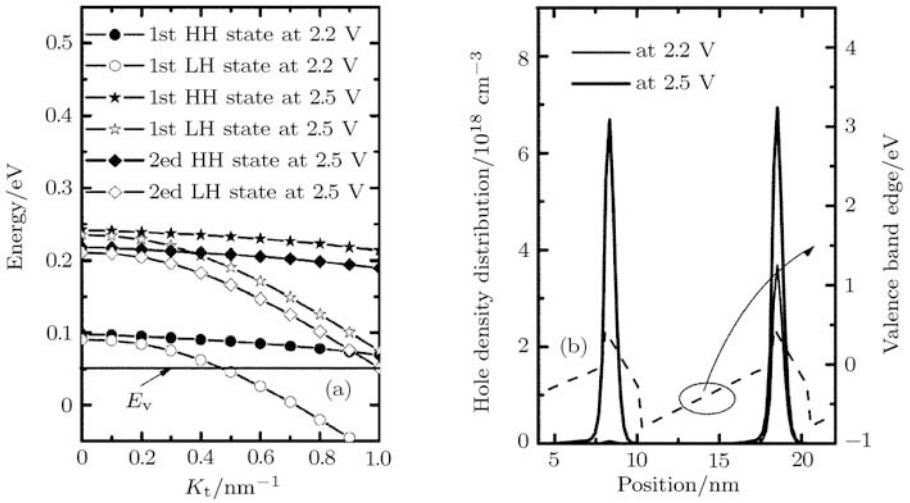


Fig. 3. (a) Subband structures and (b) hole density distributions of yellow MQW at different injection levels.

3.2. Layout of different QWs

In order to obtain white light output, the layout of the different QWs for the IMQW structure should be carefully designed. The final spontaneous emission spectrum depends mainly on the hole density distribution in valence band due to the fact that holes are more nonuniformly distributed than electron for a given injected carrier density. However, the hole distribution depends on both the band gap width of well layer and the sequence of different QWs. In the IMQW structure the QWs with larger band gap width are more difficult to obtain the hole distribution and the QWs close to P-region have a higher probability to obtain the hole distribution.[22] As a result, the IMQW structures in which the blue QWs are close to the P-region and the yellow QWs are close to the N-region have a high opportunity to obtain enough blue and yellow light emissions for white light mixing.

Figure 4 indicates the spontaneous emission spectra of the IMQW structures with different fractions of the blue and the yellow QWs at the same injection level. The layout A for IMQW structure has one yellow QW and two blue QWs, layout B has one yellow QW and one blue QW, and layout C has two yellow QWs and two blue QWs. The well material components and well width for each type of QWs are the same as the above mentioned and the thickness of the barrier is 8nm for the three IMQW structures. In order to obtain white light emitting the nonuniform hole distributions in the different QWs for IMQW structure play important roles.

As seen in Fig. 4(a), the IMQW structures with layout B and layout C have not enough blue light emissions and only the IMQW structure with layout A has enough blue and yellow light in the spontaneous emission spectrum for the white light mixing . The above

conclusion shown in Fig. 4(a) can be explained by the carrier density distribution in active region of the IMQW structure shown in Fig. 4(b). For the IMQW structures with layout B and layout C, there are much less holes distributed in the blue QWs than yellow QWs and electrons are almost uniformly distributed, which accords with the above conclusion.

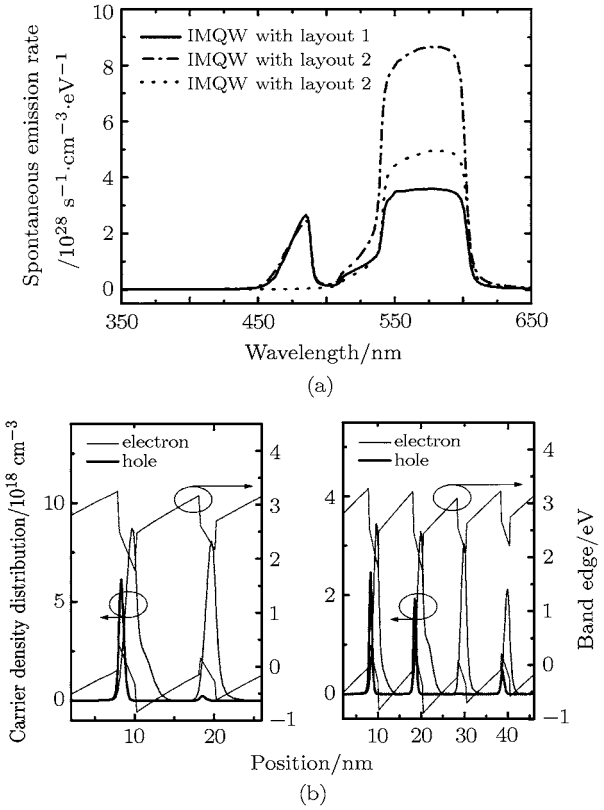


Fig. 4. (a) Spontaneous emission rates and (b) hole density distributions of the IMQW structure with different layouts.

3.3. Thickness of barrier between different QWs

The spontaneous emission spectra of the above IMQW structures composed of two blue QWs and one yellow QW with different thicknesses of barriers between blue and yellow QWs at the same injection level are plotted in Fig. 5(a). The simulation result indicates that the blue light emission increases and the yellow light emission decreases with the increase of barrier thickness between different QWs. This is because the hole in the IMQW structure with a thinner barrier has a higher probability to transport and tunnel into yellow QWs, which is in accordance with experimental result in Ref. [23]. Figure 5(b) displays the hole density distribution in active region of the IMQW structure with 8nm and 12 nm of barrier thickness. It can be seen from Fig. 5(b) that with the increase of barrier thickness the hole distribution in the blue QWs increases and the hole distribution in the yellow QW decreases, which is consistent with the above discussion about the spontaneous emission spectra.

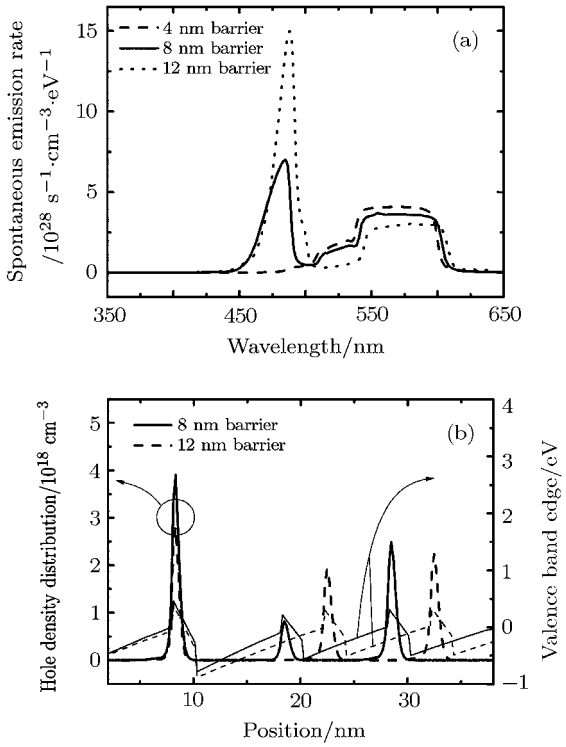


Fig. 5. (a) Spontaneous emission rates and (b) hole density distributions of the IMQW structures with different thicknesses of the barrier between different QWs.

The mixture from blue and yellow colours in an appropriate intensity ratio will fall at D_{65} used as a white light reference on the Commission International de l'Eclairage (CIE) chromaticity diagram. The spontaneous emission spectra of the IMQW structure having an 8nm barrier thickness between different QWs at different bias voltages are shown in Fig. 6(a) and indicate that almost only the intensity of blue light changes with the injection level which can simplify the adjustment of intensity ratio. The hole distribution of the middle blue QW increases obviously with the increase of injection level shown in Fig. 6(b), which is the main reason why the blue light intensity varies. Then, an appropriate intensity ratio of blue and yellow light is obtained by adjusting injection level.

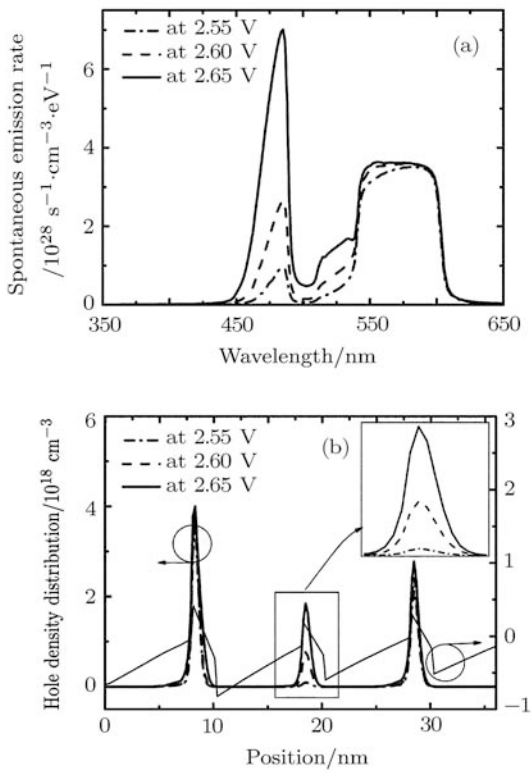


Fig. 6. (a) Spontaneous emission rates and (b) hole density distributions of the IMQW structure with an 8 nm thick barrier between different QWs.

Figure 7 exhibits the spontaneous emission spectrum of such an IMQW structure under 2.6 V of applied voltage and its comparison with emission spectrum of blackbody. The simulation result indicates that the spontaneous emission spectrum of such an IMQW structure at an appropriate injection level is close to that of nearly white light emission.

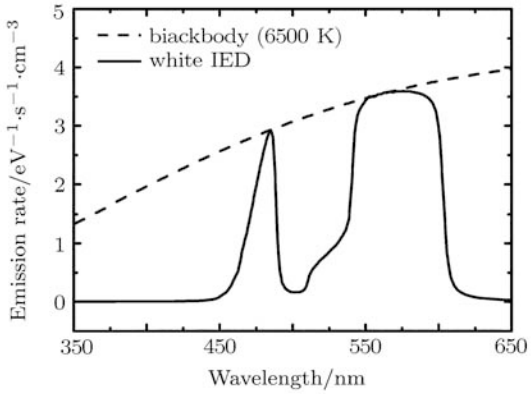


Fig. 7. Spontaneous emission rate of the IMQW structure at 2.6 V of applied voltage and emission spectrum of blackbody.

4. Conclusion

GaN-based IMQW structures for dichromatic white LEDs are optimized and the spontaneous emission properties of the IMQW structure are studied by employing a newly developed theoretical model. We theoretically demonstrate that the IMQW structure can generate nearly white light emissions by adjusting the design parameters, such as material component and well width, layout of different QWs and the thickness of barrier between different types of QWs. The simulation result shows that with the increase of barrier thickness between different QWs the blue light emission increases and the yellow light emission decreases. For the dichromatic white LEDs the GaN-based IMQW structure can be composed of two QWs emitting blue light at 485 nm wavelength, and one QW emitting yellow light at 585 nm wavelength, with each QW being 2 nm thick.

References

[1] Kim J S, Jeon P E, Choi J C, Parka H L, Mho S I and Kim G C 2004 *Appl. Phys. Lett.* **84** 2931
[2] Wu H, Zhang X M, Guo C F, Xu J, Wu M M and Su Q 2005 *IEEE Photonics Technol. Lett.* **17** 1160
[3] Sheu J K, Chang S J, Kuo C H, Su Y K, Wu L W, Lin Y C, Lai W C, Tsai J M, Chi G C and Wu R K 2003 *IEEE Photonics Technol. Lett.* **15** 18
[4] Wang Z J, Li P L, Yang Z P, Guo Q L and Li X 2010 *Chin. Phys.* B **19** 017801
[5] Wei X D, Cai L Y, Lu F C, Chen X L, Chen X Y and Liu Q L 2009 *Chin. Phys.* B **18** 3555
[6] Guo X Y, Graff J W and Schubert E F 2000 *Proc. SPIE* **60** 3938
[7] Shi J W, Huang H Y, Wang C K, Sheu J K, Lai W C, Wu Y S, Chen C H, Chu J T, Kuo H C, Lin W P, Yang T H and Chyi J I 2006 *IEEE Photonics Technol. Lett.* **18** 2593
[8] Park I K, Kim J Y, Kwon M K, Cho C Y, Lim J H and Park S J 2008 *Appl. Phys. Lett.* **92** 091110
[9] Sheu J K, Pan C J, Chi G C, Kuo C H, Wu L W, Chen C H, Chang S J and Su Y K 2002 *IEEE Photonics Technol. Lett.* **14** 450
[10] Lu H M, Chen G X and Jian S S 2009 *Chin. Phys. Lett.* **26** 087803
[11] Park S H and Chuang S L 1998 *Appl. Phys. Lett.* **72** 3103
[12] Park S H and Chuang S L 2000 *Appl. Phys. Lett.* **76** 1981
[13] Bernardini F and Fiorentini V 1999 *Phys. Stat. Sol.* (b) **216** 391
[14] Chuang S L and Chang C S 1996 *Phys. Rev.* B **54** 2491
[15] Chuang S L 1996 *IEEE J. Quantum Electron.* **32** 1791
[16] Chuang S L and Chang C S 1997 *Semicond. Sci. Technol.* **12** 252
[17] Chuang S L 1995 *Physics of Optoelectronic Devices* (New York: Wiley) p263
[18] Adachi S 1989 *Phys. Rev.* B **39** 12612
[19] Piprek J 2003 *Semiconductor Optoelectronic Devices* (San Diego: Academic Press) p34
[20] Rinke P, Scheffler M, Qteish A, Winkelnkemper M, Bimberg D and Neugebauer J 2006 *Appl. Phys. Lett.* **89** 161919
[21] Vurgaftman I and Meyer J R 2003 *J. Appl. Phys.* **94** 3675
[22] David A, Grundmann M J, Kaeding J F, Gardner N F, Mihopoulos T G and Krames M R 2008 *Appl. Phys. Lett.* **92** 053502
[23] Liu J P, Ryou J H, Dupuis R D, Han J, Shen G D and Wang H B 2008 *Appl. Phys. Lett.* **93** 021102